



Article

Photoprotective Steering of Provitamin D₃ Photochemistry by Phenylalanine in Solution

Gordon A. Ochsner, Jaren S. Meikle and Jacob C. Dean *^{ID}

Department of Chemistry and Physics, Southern Utah University, Cedar City, UT 84720, USA; gtochsner1@gmail.com (G.A.O.); jarenmeikle@gmail.com (J.S.M.)

* Correspondence: jacobdean@suu.edu

Abstract: Provitamin D₃ is the biological precursor to naturally formed vitamin D₃ in humans, and its conversion is initiated via photoexcitation by near ultraviolet light. Following an initial photolysis, the primary intermediate, known as previtamin D₃, is prone to light-induced isomerization or recyclization, which creates byproducts that limit the desired final thermal conversion to vitamin D₃. The branching of the photochemical reaction is highly wavelength-dependent, whereby excitation toward the blue edge of the provitamin D₃ absorption spectrum tends to terminate the reaction with the most undesired tachysterol byproduct and the lowest previtamin D₃ concentration. In this work, the influence of introducing the natural amino acid phenylalanine as an excitation energy donor to the photochemical reaction is investigated. We find that the incorporation of phenylalanine into provitamin D₃ solution results in greater intermediate concentrations and prolonged lifetimes of the desired previtamin D₃ while simultaneously reducing the final concentration of tachysterol when exposing the solution to wavelengths at the blue edge of the provitamin D₃ spectrum. The results, coupled with quantum chemical analysis, suggest that phenylalanine indeed helps to funnel energy from shorter wavelengths more effectively into the provitamin D₃ precursor, while simultaneously screening those wavelengths from direct excitation, which otherwise leads to enhanced concentrations of tachysterol byproduct at the expense of previtamin D₃.

Keywords: provitamin D photochemistry; 7-dehydrocholesterol; photoprotection; resonance energy transfer



Citation: Ochsner, G.A.; Meikle, J.S.; Dean, J.C. Photoprotective Steering of Provitamin D₃ Photochemistry by Phenylalanine in Solution. *Photochem.* **2023**, *3*, 477–494. <https://doi.org/10.3390/photochem3040029>

Academic Editor: Rui Fausto

Received: 15 October 2023

Revised: 11 November 2023

Accepted: 20 November 2023

Published: 28 November 2023



Copyright: © 2023 by the authors. Licensee MDPI, Basel, Switzerland. This article is an open access article distributed under the terms and conditions of the Creative Commons Attribution (CC BY) license (<https://creativecommons.org/licenses/by/4.0/>).

1. Introduction

Vitamin D₃ is a crucial nutrient for maintaining bone density [1–4] and regulating mood in humans [5,6]. It is a fat-soluble sterol that can be endogenously formed [7,8] or supplemented through a nutrient-rich diet [9,10]. Since a sufficient supply of vitamin D₃ can be synthesized with light alone to support physiological function, this disqualifies it as a proper vitamin by definition [11]. In the human body, 7-dehydrocholesterol, also known as provitamin D₃ (Pro-D), is a necessary intermediate in the cholesterol biosynthesis pathway [12] and its secondary use is as the primary vitamin D₃ precursor [13]. Provitamin D₃ has a characteristic steroid base with a long alkyl chain (Figure 1) that helps stabilize its presence in lipids [14]. Lipids often depend on steroids to modulate their fluidity, and when a specific lipid bilayer requires structural support, steroids are sent to provide it, making lipids the primary region where Pro-D is found within human skin [14–16]. The concentration of Pro-D within lipid bilayers of the stratum spinosum and stratum basale regions of the epidermis ranges between 20–100 µg/cm² of the lipid layer [4]; however, the amount of Pro-D present in individuals can vary due to several factors, including age, diet, environment, and general lifestyle [17,18].

As shown in Figure 1, the process of converting Pro-D to vitamin D₃ begins with exposure to UV light. The excited Pro-D, following a $\pi\rightarrow\pi^*$ transition, rapidly undergoes photolytic ring opening at the cyclohexadiene chromophore, resulting in the formation

of the metastable triene intermediate, previtamin D₃ (Pre-D) [19,20]. The near-ultrafast timescale for the photochemical ring-opening of Pro-D→Pre-D has been found to be 1–2 ps, according to ultrafast transient absorption and circular dichroism spectroscopy [21,22]. However, the decay of excited Pre-D is biexponential, with a seemingly parallel ~0.5 ps component associated with internal conversion to the ground state, resulting in a final fluorescence quantum yield of $\sim 3 \times 10^{-4}$ [21,23]. It should be noted, however, that more recent transient absorption and high-level theoretical treatments of the excited-state dynamics have shown that the biexponential decay actually stems from nonequilibrium dynamics along the ring-opening coordinate where the excited population oscillates across the S₀/S₁ coupling region [24,25]. While these dynamics result in biexponential excited-state decay as measured in the experiment, the physical picture precludes the concept of two exclusive parallel pathways for ring-opening and internal conversion.

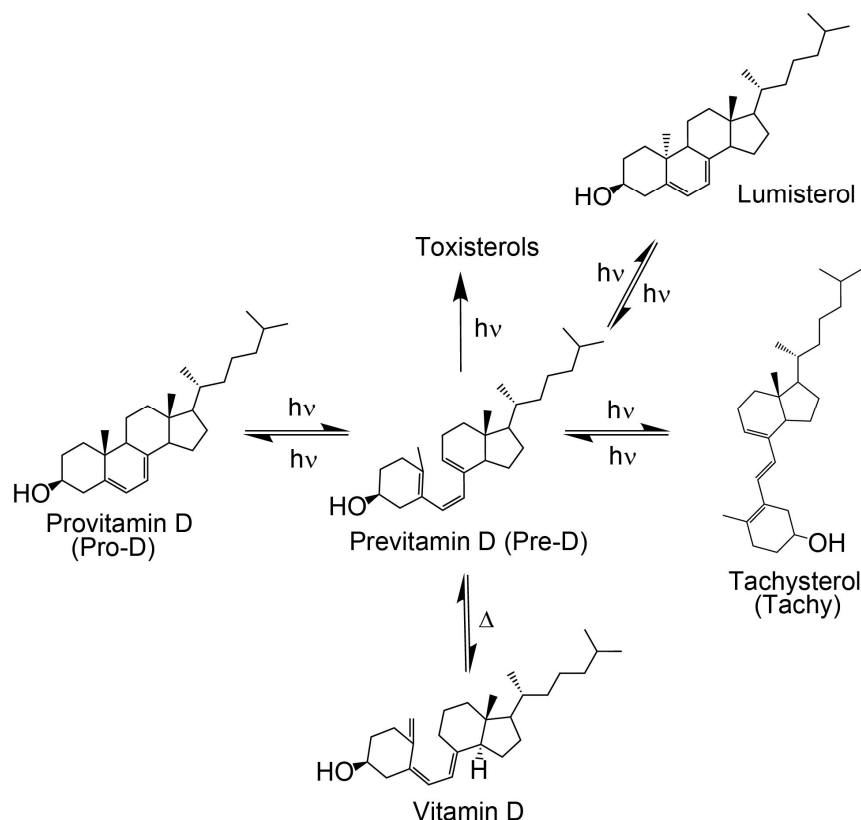


Figure 1. Photochemical pathways following provitamin D₃ photoexcitation.

The photochemical Pre-D intermediate is considered a secosterol, which refers to a sterol backbone that has opened its ring, conferring significant conformational flexibility compared to its Pro-D counterpart. As such, following its rapid formation, it is prone to further thermal and photochemical isomerization reactions, resulting in a wide variety of tertiary structures, one of which is the desired vitamin D (Figure 1) [19,20,26]. The mechanisms for those reactions have been well studied and documented [23,27–30]. Briefly, the initial Pre-D conformation following photolysis adopts a gZg configuration (or cZc in 2D) according to the relative orientations of the outer double bonds about the central double bond [23,30,31]. The hot ground-state gZg conformer then thermalizes into an equilibrium distribution of cooled gZg and tZg (following a nominally *cis*→*trans* isomerization about the first single bond), favoring the lower free energy tZg conformer in solution [17,30,32]. Notably, the dominant tZg-Pre-D absorbs blue of the Pro-D absorption spectrum (Figure 2) with wavelengths shorter than 260 nm, while the gZg conformer absorbs red around 300 nm [17,30–32]. Vitamin D is finally produced by the thermal rearrangement of the gZg Pre-D conformer in vivo [16,33].

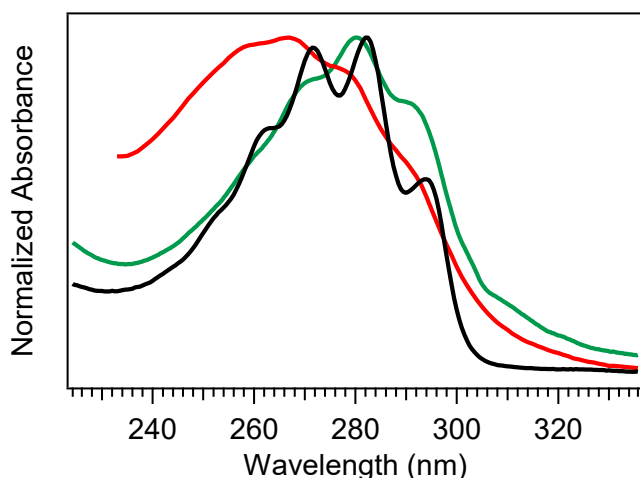


Figure 2. Absorption spectra of provitamin D₃ (black), previtamin D₃ (red), and tachysterol (green). The previtamin D₃ spectrum was extracted following a long-time exposure of Pro-D to 294 nm light, while tachysterol was extracted following a long-time exposure of Pro-D to 258 nm light. The spectra for Pre-D and Tachy are therefore treated as approximate, as the species have not been completely isolated.

If the ground state Pre-D is continuously exposed to UV light, it is susceptible to further undesired photochemistry leading to lumisterol, toxisterols (irreversible), and the main photoproduct tachysterol (Tachy) [19,20,28,31]. Figure 2 shows a comparison of absorption spectra for Pro-D, Pre-D, and Tachy in methanol. Extraction of the Pre-D spectrum in Figure 2 was done by long-time exposure to 294 nm light, while Tachy was collected following long-time exposure to 258 nm. We note that, by comparison to other spectra recorded under similar conditions [30,32,34], the Pre-D spectrum in the figure contains a trace population of lumisterol seen from the hint of structure underneath the otherwise broad Pre-D profile.

It has been found that Tachy preferentially accumulates from the *tZg*-Pre-D form due to less overlap of the *tZg*-Pre-D absorption spectrum with Tachy and Pro-D. This essentially traps a photostationary population of Tachy, while exposure wavelengths further red access the reverse reactions Tachy → Pre-D and Pre-D → Pro-D, which recycles the precursors and therefore maximizes equilibrium Pre-D formation. The reverse reactions leading to ring closure (Pro-D formation) at red wavelengths can be rationalized by the *gZg* absorption in that region, which poises the Pre-D triene optimally for reformation of the diene ring. Importantly, rearrangement to the desired vitamin D₃ product from Pre-D is the only pathway not achieved photochemically—therefore, maximizing a steady-state population of Pre-D should also maximize final vitamin D₃ production *in vivo*.

Taking these factors altogether, the broad, conformationally-heterogeneous Pre-D absorption spectrum along with the unique absorption spectra of secondary products leads to significant wavelength dependence in the photostationary populations of all species possible in the photochemical reaction. Norval et al. [28] nicely summarized the wavelength dependence on quantum yields for the formation of each species by compiling results from several seminal works. As previously suggested, it is found that when Pro-D is illuminated at the blue edge of its S₀–S₁ absorption band, the steady-state concentration of Tachy is maximal, while the 290–300 nm region primarily favors Pre-D. Specifically, at 254 nm exposure, the Tachy/Pre-D fraction was found to be 3.6, while at 300 nm, it was 0.40 [28]. Again, the yield dependence on wavelength can be rationalized by the conformational distribution of Pre-D and their absorption regions. With this in mind, several studies have investigated the effect of environment on the wavelength sensitivity to product yield. Interestingly, the reaction is very insensitive to solvent polarity, showing similar Pre-D formation kinetics and product branching in heptane and alcohols, for example. However, incorporation of Pro-D into other media such as liquid crystals [31,35], silica

gel [31,36], and lipid bilayers [32] was found to affect photostationary populations, more often inhibiting Tachy formation relative to Pre-D through conformational effects fostered by van der Waals interactions with the materials. These effects *in vivo* significantly enhance vitamin D₃ production, as it is believed that the gZg-Pre-D form ultimately precedes thermal conversion to vitamin D₃ [33,37].

The conformationally-driven optimization of vitamin D production by explicit interactions with heterogeneous materials suggests then that aggregation of Pro-D by a single molecule in solution may similarly steer the product branching of its photochemistry and optimal Pre-D production, presuming the appropriate interaction(s). In addition, selection of a UVB chromophore as the aggregate partner could achieve a similar result by altering the action spectrum and potentially engaging in Förster resonance energy transfer (FRET) with Pro-D as its energy acceptor. In this work, we aim to investigate these effects by comparing the spectral evolution of Pro-D with and without the presence of a FRET donor in solution. Further, the wavelength dependence of the photoconversion of Pro-D to time-dependent populations of Pre-D and Tachy is also compared in order to address the factors responsible for any changes in the photochemical mechanism due to the presence of the donor compound. By utilizing a single small molecule as the “substrate” for Pro-D, insights into the particular chemical driving forces that optimize vitamin D production *in vivo* can be closely examined. Namely, we seek to explore the following questions: (1) is the optimal condition for maximizing vitamin D production primarily restriction of the Pre-D conformation/flexibility? (2) Does screening shorter wavelengths of light by other UV absorbers help optimally steer Pre-D formation? (3) Can a FRET donor enhance efficiency of Pre-D formation by down-converting parasitic high energy UV light to excitation wavelengths which favor Pre-D?

The selection of a binding partner must be made judiciously to satisfy several criteria that are compatible with Pro-D. Namely, structural properties must first be considered to generate the potential for binding in a well-dissolved solution, and secondly, the spectral characteristics should enable the capacity for FRET toward the Pro-D acceptor. Furthermore, the compound should be highly photostable in the region 220–320 nm. Here, we have chosen the natural amino acid phenylalanine (Phe) due to its similar solubility properties as Pro-D and its incorporation of a hydrogen bond donor and acceptor. In addition, the incorporation of a phenyl ring yields an absorption just blue of Pro-D peaking at 258 nm with a fluorescence spectrum that yields optimal overlap with the Pro-D absorption spectrum to ensure energy conservation in the FRET process (i.e., spectral overlap). To demonstrate this FRET compatibility, the Phe absorption (blue) and fluorescence (red) spectrum are shown in Figure 3 against the Pro-D absorption spectrum (black) in methanol, along with the spectral overlap function (shaded green) plotted below. In Figure 3, the spectral overlap function is notably found almost exclusively in the region overlapping the gZg Pre-D absorption red of 260 nm. Finally, Phe is a ubiquitous natural amino acid and has many relevant physiological functions, including its role in anchoring proteins and enzymes to lipid bilayers. Such a case would bring the Phe residue within a protein in proximity to the Pro-D imbedded in the lipid bilayer.

In what follows, we compare the evolution of the UV-vis absorption spectrum of a Pro-D solution in the absence of Phe to one incorporating Phe and utilize the wavelength dependence of product branching to aid in interpreting the role of Phe on the photochemical mechanism. We find that the presence of Phe inhibits Tachy buildup, while simultaneously generating a prolonged population of Pre-D. Global spectral analysis was performed to evaluate the kinetics of the reaction for each case, and high-performance liquid chromatography (HPLC) was used to estimate the final Tachy and Pre-D product yields. Quantum chemical calculations were performed to predict the binding properties of various Pro-D•••Phe dimer conformations, and FRET analysis was done to predict energy transfer properties between them.

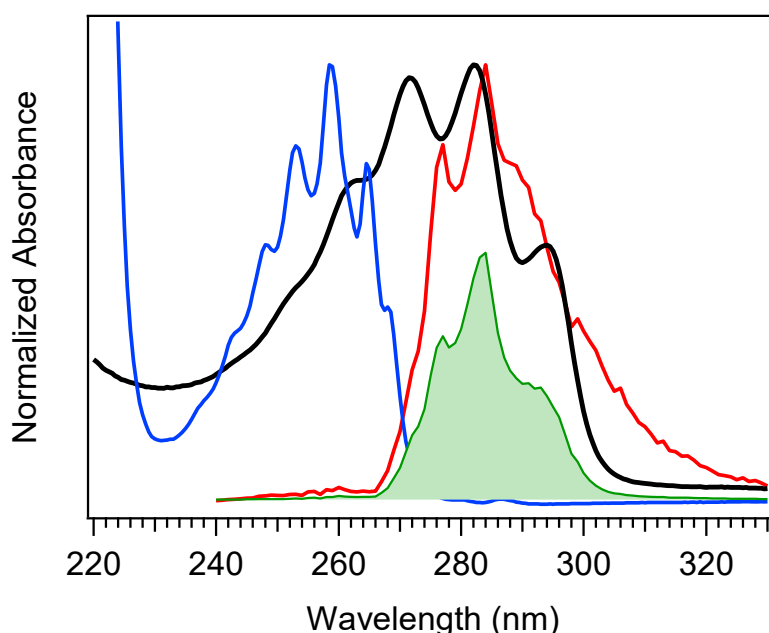


Figure 3. Absorption spectrum of Pro-D (black) and Phe (blue), along with the Phe fluorescence spectrum (red), and the spectral overlap function in shaded green. The spectral overlap function has been calculated according to Scholes [38], but the scale shown is arbitrary.

2. Methods

2.1. Experimental Methods

7-dehydrocholesterol (Pro-D) was purchased from Sigma-Aldrich (St. Louis, MO, USA) at a purity of $\geq 95.0\%$ and used without further purification. L-phenylalanine (Phe) was purchased from Alfa Aesar (Haverhill, MA, USA) at a purity of 99% and used without purification. Pro-D concentrations were kept at $1-2 \times 10^{-4}$ M for all measurements, while Phe was kept to $\sim 2 \times 10^{-3}$ M to yield a similar total absorbance as Pro-D in a 1:1 mixture by volume. Methanol was used as the solvent for all solutions reported. UV-visible absorption measurements were carried out on a Cary 3500 UV-vis spectrophotometer (Agilent, Santa Clara, CA, USA). The excitation source used to irradiate the sample throughout the photochemical reaction was a Xe-arc lamp/monochromator module of a Photon Technology International (PTI) fluorometer with an output slit width of 1.0 mm, yielding a final wavelength resolution of ~ 5 nm FWHM (Figure S1). The sample was continuously stirred in a 1 cm quartz cuvette. The power incident on the sample was kept at $0.70 \mu\text{W}$, and a slit at the Xe-arc lamp output was used to modulate the final power at the sample and kept consistent across excitation wavelengths. In order to highlight changes in the UV-vis spectrum occurring throughout the progress of the reaction, difference absorption spectra, $\Delta A(t) = A(t) - A(0)$, were analyzed and reported here, where the initial spectrum prior to irradiation at $t = 0$ was subtracted from each absorption spectrum at irradiance time, t . In this way, losses in absorbance are displayed as negative signals, while growth is displayed as positive. Global analysis of the time-resolved absorption data was performed using the Glotaran program [39]. Photochemical experiments were carried out at excitation wavelengths of 258 nm and 294 nm for Pro-D:Phe mixtures, as well as Pro-D solutions for an active comparison of the effect of Phe on the reaction and the subsequent wavelength dependence. Concentrations and excitation power were kept consistent for those measurements.

HPLC measurements of the solutions before UV exposure and at the end of an irradiance experiment were carried out on an Agilent 1200 system coupled with diode-array detection (DAD) for UV-vis assignments of each elution. An isocratic mixture of acetonitrile:methanol:water at 24:69:7 (%v) was used as the mobile phase through a $3.5 \mu\text{m}$ Agilent Eclipse Plus C18 column to achieve adequate separation, with a flow rate of 0.50 mL/min .

Estimates on the relative concentrations and product fractions were found by integrating each individual elution in the chromatogram measured at 280 nm, where Pro-D, Pre-D, and Tachy all generate significant absorptivity. Each chromatogram was fit to a sum of gaussian functions representing each elution to appropriately integrate the total absorbance throughout each elution despite some overlap. Division of each species' approximate molar extinction coefficient at that wavelength [28] by the total absorbance found from integration yielded an estimate of the concentration of each species.

2.2. Computational Methods

All quantum chemical calculations were performed in the Gaussian 16 suite [40] using density functional theory (DFT) at the M06-2X/6-31+G(d) level of theory, including implicit solvation in methanol approximated using the polarizable continuum model. Pro-D, Phe, and all Pro-D•••Phe van der Waals dimer geometries were optimized, followed by harmonic vibrational frequency calculations. The Gibbs free energies for those structures were used to predict binding free energies for approximately 40 Pro-D•••Phe dimer structures, which were the lowest energy configurations generated from a conformational search within the Macromodel program [41] using the MMFF force field. Binding free energies are calculated by subtracting the Gibbs energy from the sum of individual Pro-D and Phe structures (with similar starting conformation) from the aggregate:

$$\Delta G_{binding} = G_{Pro-D \bullet\bullet\bullet Phe} - [G_{Pro-D} + G_{Phe}] \quad (1)$$

Importantly, Gibbs energies were taken from structures calculated at the same level of theory so that the relative energy scale is consistent.

3. Results

The absorption spectra for Phe and Pro-D in methanol are shown in Figure 3, displaying a λ_{max} of 258 nm and 282 nm, respectively. The Phe spectrum spans from ~235 to 275 nm, while the spectrum of Pro-D is broader, ranging from 240 to 300 nm for its first electronic transition. Notably, the wavelength region of Phe, which covers the blue edge of Pro-D's, yields a significant Tachy concentration from Pro-D in the absence of Phe. However, the first vibronic band of Pro-D is found at 294 nm, significantly red-shifted from Phe in a region where Pre-D is preferentially formed. With that in mind, four distinct irradiance studies are reported in what follows, associated with two excitation wavelengths. The first set is associated with an irradiance wavelength of 294 nm, exposing a pure Pro-D solution compared against that of a 1:1 mixture of Pro-D:Phe. The second set is to the blue at 258 nm (Phe λ_{max}) of the same pair of starting solutions. The effect of Phe on the Pro-D spectral evolution and its wavelength dependence are evaluated through the time-resolved difference absorption spectra, which conveniently subtract Phe's contribution to the total absorption spectrum. Its complete absence in the ΔA spectra for the mixtures further indicates its high photostability, leaving only changes to the Pro-D photochemistry represented in the spectra.

The spectral evolution of a Pro-D solution irradiated with 294 nm light for a total of 90 min is shown in Figure 4a,b. Immediately, depletion of Pro-D signatures is detected and reaches a minimum ΔA around 30 min of exposure time. Throughout the experiment, a broad feature to the blue ranging from 240 to 270 nm gradually grows in and reaches up to 0.13 optical density (OD) at the end of the experiment. In a similar way, another broad induced absorption peaks at 303 nm and trails off past 320 nm. The feature is distorted due to the negative Pro-D signals, but comparison to the steady-state absorption spectra (top) suggests that the combination of these broad signals arise from a growing Pre-D population with traces of Tachy. The blue-most features are particularly distinguishable as Pre-D since the Tachy absorption approaches a minimum there.

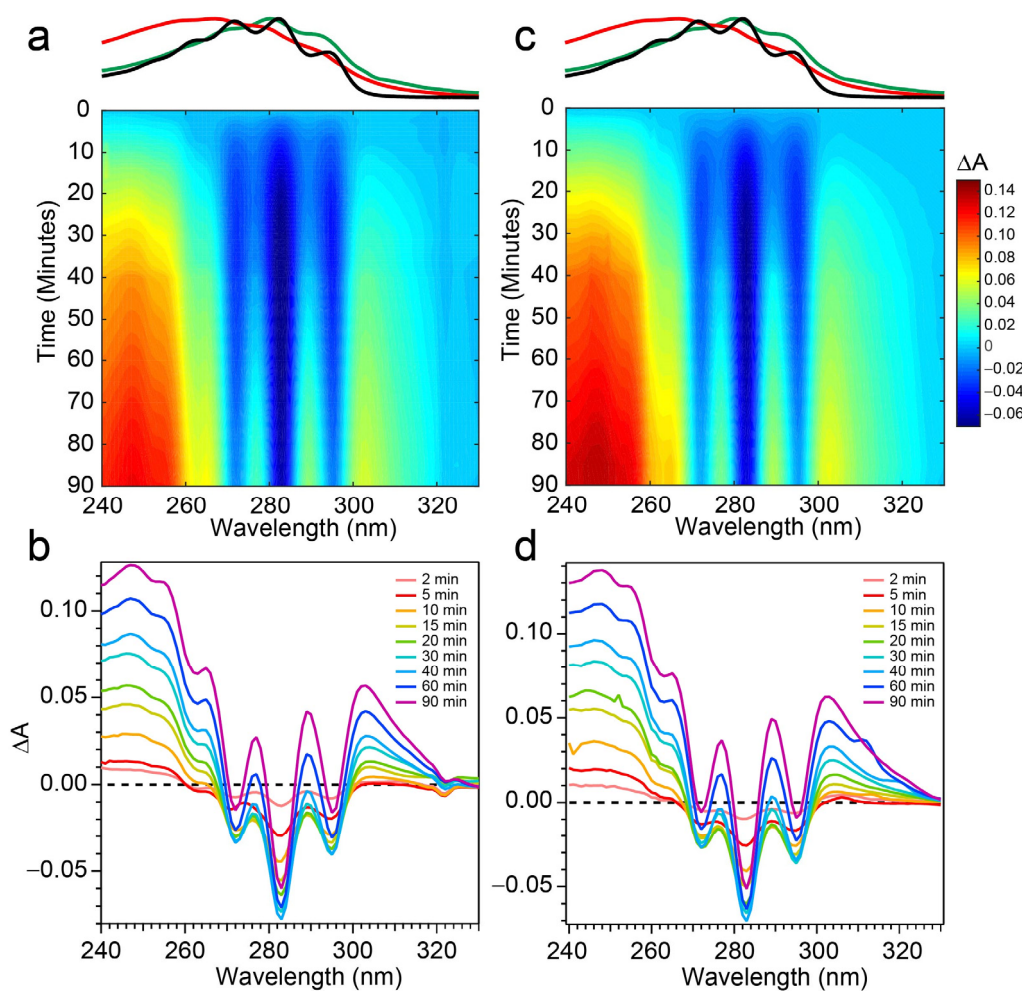


Figure 4. Difference absorption spectra at 294 nm excitation wavelength for (a,b) Pro-D solution and a (c,d) 1:1 Pro-D:Phe mixture. Approximate absorption spectra of Pro-D, Pre-D, and Tachy are shown at the top, for reference, with the same color scheme shown in Figure 2.

The transients taken from four different wavelengths are shown as open triangles in Figure 5a. At 283 and 294 nm, traces of the Pro-D depletion are clearly shown as an early-time exponential decay, before “recovering” and gradually increasing throughout the rest of the experiment. The slow growth at those wavelengths tracks similarly with the growth rate of features to the blue (245 nm) and red (305 nm) of the Pro-D absorption, indicating spectral overlap within the Pro-D absorption region and predominantly sequential kinetics of Pro-D \rightarrow Pre-D (+trace Tachy). These results are in agreement with former works that have shown that excitation at the red edge of the Pro-D absorption spectrum helps to maximize Pre-D concentration.

Figure 4c,d shows the same measurement on a 1:1 Pro-D:Phe mixture to investigate the effects of Phe’s presence in solution on the photochemical reaction. In this case, the signals and time evolution are found to be nearly indistinguishable from a Pro-D solution. A closer comparison is found by inspecting the transients (Figure 5a) where solid circles represent the mixture with Phe, and the signal progression is found to be nearly identical. Despite the parity in kinetics between the experiments, a slight difference in Pro-D concentration between the two measurements yields a minor difference in the magnitude of ΔA signals. Nevertheless, the concentration ratio for products remains very similar for the entirety of the experiment, indicating little to no effect on the photochemical mechanism by the simple presence of ground-state Phe. Importantly, 294 nm exposure excludes excitation of Phe altogether and therefore any effects of excited Phe.

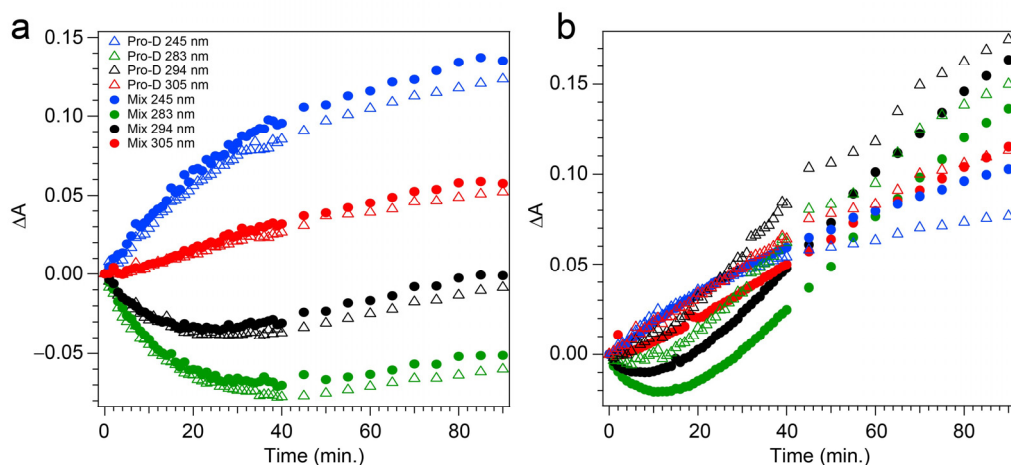


Figure 5. Experimental transients taken at 245 nm (blue), 283 nm (green), 294 nm (black), and 305 nm (red) detection wavelengths, following (a) 294 nm and (b) 258 nm light exposure. Open triangles indicate pure Pro-D solutions in methanol, while solid circles indicate 1:1 Pro-D:Phe mixtures in methanol.

To address those aforementioned exclusions in the 294 nm experiments, time-resolved absorption spectra were recorded while exposing the two samples to 258 nm light ($\text{Phe } \lambda_{\text{max}}$) of the same intensity. The results are shown in Figure 6. The wavelength dependence of the product branching is evident, as the differential spectra are remarkably different than those found in Figure 4. While the negative-going Pro-D depletion is detected at very early times in Figure 6a,b, it fades into a large growth spanning the entire 240–320 nm region, the center of which reveals vivid vibronic signatures with characteristic peaks at 300 nm, 290 nm, and 278 nm. These features are very close to the first three vibronic bands of the Tachy spectrum, and the nearly $2\times$ increase in ΔA further reinforces that assignment given the $>2\times$ molar extinction coefficient of Tachy compared to Pro-D [28]. Inspection of the transients in Figure 5b (open triangles) reiterates the dramatic variability in concentrations as a function of UV wavelength, showing very different signal evolution compared to Figure 5a. Importantly, we find a significantly faster growth at 283 and 294 nm following a brief Pro-D decay, representative of primarily Tachy formation. Similarly, the signal at 305 nm is enhanced in this experiment, again very near the first distinguishable Tachy feature. Another notable difference is that the total growth at the blue edge of the spectrum where Pre-D is identified (blue triangles) is reduced nearly a factor of two compared to 294 nm excitation, indicating less overall Pre-D formation in this case.

Repeating the same measurement on a Pro-D solution incorporating Phe rendered distinct differences in the progression of signals in the difference absorption spectrum, as well as the final signal strength (Figure 6c,d). Comparing the spectrum to the Pro-D solution reveals an apparently prolonged and more dramatic depletion of Pro-D concentration reaching a minimum ΔA around 15 min before transitioning into the buildup of product absorption throughout the remainder of the experiment. At first glance, it appears that again, Tachy formation dominates the product mixture; however, close inspection to the red and blue edge of the spectrum reveals additional signals not present in the pure Pro-D solution excited at this wavelength. Those signals can confidently be assigned to the buildup of a concomitant Pre-D population not observable without the presence of Phe.

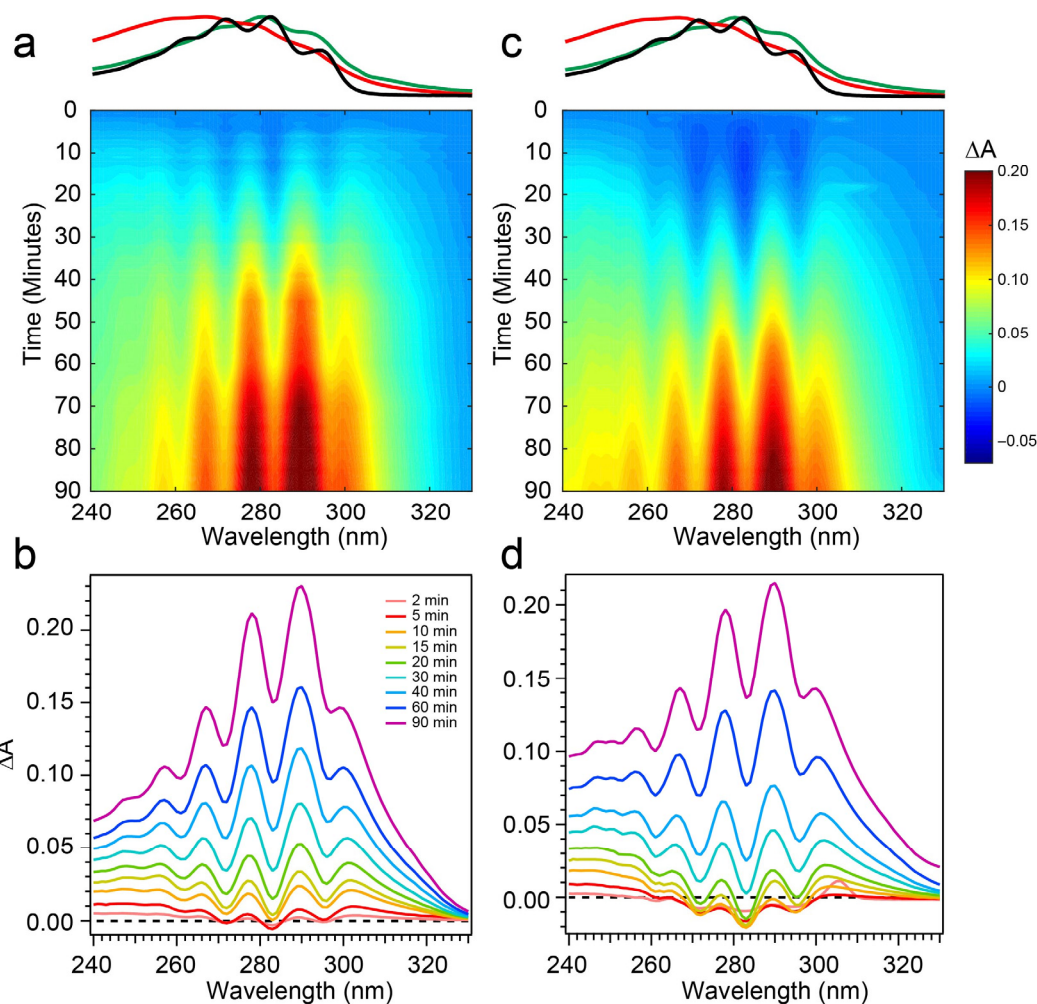


Figure 6. Difference absorption spectra at 258 nm excitation wavelength for (a,b) Pro-D solution and a (c,d) 1:1 Pro-D:Phe mixture. Approximate absorption spectra of Pro-D, Pre-D, and Tachy are shown at the top, for reference, with the same color scheme shown in Figure 2.

The prolonged decay of Pro-D, the buildup of Tachy, and the enhancement in Pre-D concentration are illuminated in a comparison of the transients taken at wavelengths characteristic of those species (Figure 5b). Most notably, the transient at 245 nm (blue) shows a difference of about 0.03 OD at 90 min, and the absorbance there is plateauing in the Pro-D solution while continuing to increase in the 1:1 Pro-D:Phe solution. Furthermore, the final Tachy absorbance is noticeably less in the mixture. While the relative absorbance of the Pre-D and Tachy features still appears to favor Tachy, it must be noted that the molar extinction coefficients of the two species are dramatically different, perhaps indicating a more significant change in their relative concentrations, comparing the two experiments.

In order to quantify the final concentrations of Pro-D products among the four photochemical experiments, high-performance liquid chromatography (HPLC) utilizing diode-array detection (DAD) was employed. Figure 7 shows the chromatograms measured at 280 nm for product solutions extracted after a 90 min illumination time for Pro-D solutions (black) and 1:1 Pro-D:Phe mixtures (red) under 294 nm (top) and 258 nm (bottom) illumination. We note that the detection wavelength is near the Tachy absorbance maximum. The slightly higher pre-illumination concentration of the Pro-D solution is again apparent in the chromatogram for 294 nm excited solutions, showing a similar difference in peak height between the pure Pro-D and Pro-D:Phe mixture for all three eluted species. However, their concentration ratios appear to remain nearly the same in agreement with difference absorption measurements (Figure 4). However, for the 258 nm illuminated solutions, a clear

decrease in Tachy is found along with a slight increase in Pre-D and Pro-D concentrations. These results are consistent across all other detection wavelengths in the DADS as shown in Figure S3 in the Supplementary Material.

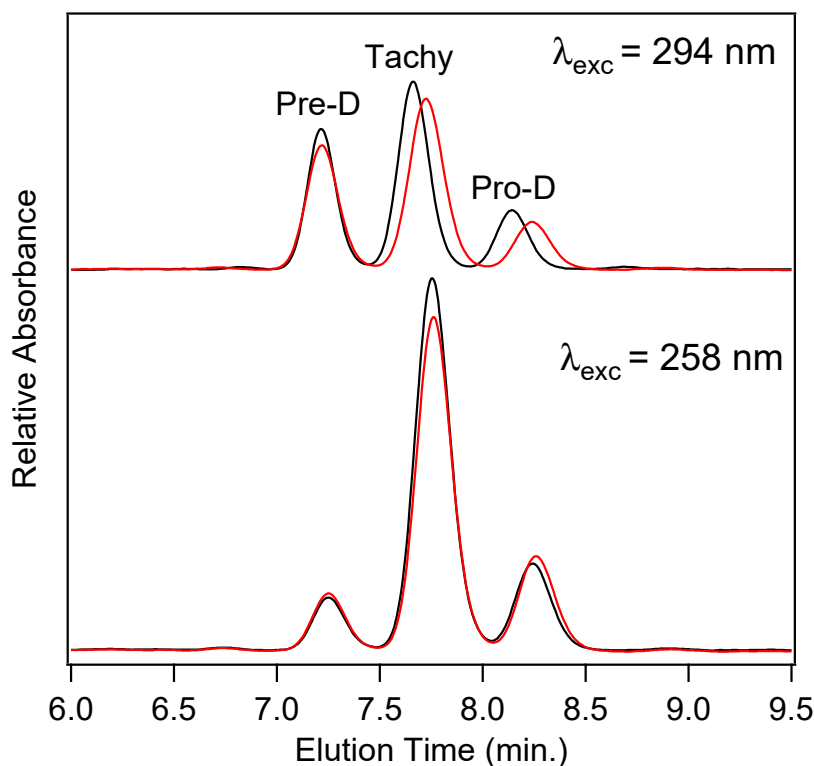


Figure 7. HPLC-DAD chromatograms for Pro-D solutions (black) and 1:1 Pro-D:Phe mixtures (red) at a detection wavelength of 280 nm. The solutions were all illuminated for a total of 90 min with the same excitation light intensity at 294 nm (**top**) and 258 nm (**bottom**).

To quantify the relative concentrations of Pre-D:Tachy in the two sets of experiments, the chromatograms were fit with a sum of three gaussians and integrated to yield a total absorbance for each species, then corrected for their approximate molar extinction at 280 nm according to Norval et. al. [28] These fits can be found in the Supplementary Material in Figure S3. We find a [Pre-D]:[Tachy] ratio of 1.96 and 1.92 for the Pro-D and 1:1 Pro-D:Phe mixtures, respectively, at 294 nm excitation wavelength, yielding a percent difference of -1.89% . However, for solutions illuminated at 258 nm, a [Pre-D]:[Tachy] ratio of 0.36 and 0.458 were found, respectively, yielding a $+27.2\%$ difference in favor of Pre-D in the mixture. Taking these results together, it would seem that the presence of Phe enables a reduction of Tachy generation, or at least a slowdown of Tachy formation prior to reaching a photostationary state. The outcome is, therefore, a simple form of “photoprotection” of the metastable Pre-D intermediate necessary for eventual vitamin D formation. The potential mechanism of this photoprotection is explored in what follows.

4. Discussion

4.1. Global Analysis and Kinetics

The changes in difference absorption spectra throughout the course of the photochemical reaction due to the presence of Phe, along with the differences in final concentrations of Pre-D and Tachy found through HPLC analysis, warrant a thorough kinetic analysis to investigate potential mechanisms of “photoprotection” apparent in those results. To do so, global analysis was performed on the time-dependent absorption spectra recorded for 258 nm illumination, given that only significant alterations were found in those data. The data were modeled with a sequential kinetic scheme, and the evolution-associated spectra (EAS) and the rate constants, k , and time constants, τ , are given in Figure 8 and Table 1,

respectively. The sequential model incorporating three components yielded an excellent fit for both experiments, and a comparison of those fits to the transients shown in Figure 5b is given in Figure S4 of the Supplementary Material.

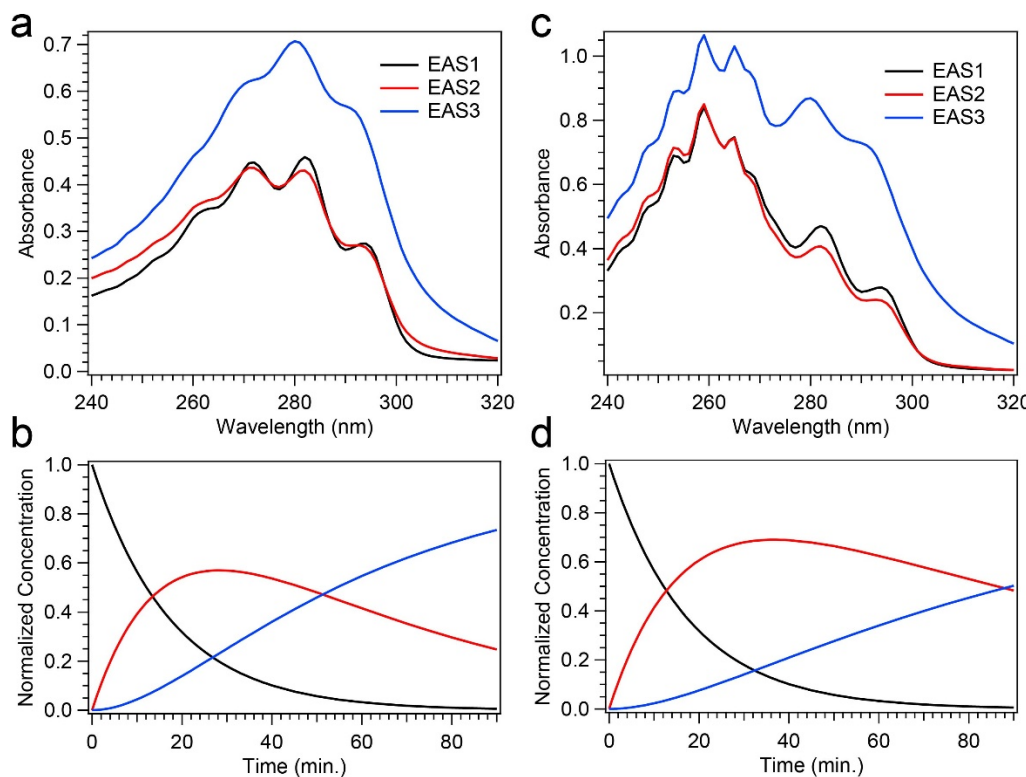


Figure 8. Global analysis results from time-resolved absorption spectroscopy. (a,c) Evolution-associated spectra (EAS) for Pro-D (a) and Pro-D:Phe (c) solutions. (b,d) Kinetics derived from the global sequential model for Pro-D (b) and Pro-D:Phe (d); the colors of traces match the appropriate EAS in (a,c).

Table 1. Rate and time constants extracted from global analysis of absorption data for Pro-D and a Pro-D:Pre-D mixture.

	Pro-D		Pro-D:Phe	
	k (min^{-1})	τ (min)	k (min^{-1})	τ (min)
EAS 1	0.057	17.5	0.057	17.5
EAS 2	0.020	50.3	0.010	99.3
EAS 3	3.7×10^{-4}	2.7×10^3	3.7×10^{-4}	2.7×10^3

The EAS for the Pro-D solution shown in Figure 8a all bear significant resemblance to spectra yielded for Pro-D, Pre-D, and Tachy, respectively. EAS1, which decays with a time constant of 17.5 min, strongly resembles the Pro-D spectrum, indicating a decay of the Pro-D concentration into EAS2. EAS2 shows an increase in absorbance both at the red and blue edge of the spectrum, coupled with a broadening about the vibronic features of Pro-D and a concomitant decrease in absorbance there. These signatures can be assigned to the intermediate Pre-D species, and it decays with a time constant of about 50 min. Finally, EAS3 is confidently assigned to Tachy, and the lack of any other notable features therein indicates its predominance in the product yield at 90 min. We note that the time constant for EAS3 is significantly longer than the experiment, meaning no decay is observed. The resulting kinetics from the global model are shown in Figure 8b.

Figure 8c,d shows the global analysis results for the Pro-D:Phe mixture. Since the absorption spectrum must be used for global analysis instead of the absorbance difference,

ΔA , the Phe spectrum in the 240–270 nm region is present in all EAS since it remains stable throughout the experiment (no decay). With that in mind, EAS1 and EAS2 display similar characteristics to those in the Pro-D solution and can be assigned once again to Pro-D and Pre-D, respectively. Again, EAS2 shows a broadening in the Pro-D spectral region along with a slight increase in absorbance to the red and blue as expected. Finally, EAS3 also shares a resemblance to the Pro-D solution, in that characteristic Tachy peaks at 280 nm and 291 nm are found, along with a strong increase in absorbance in that region. Despite most of the spectral similarities, there are notable differences observed. Firstly, while it is difficult to compare the 240–270 nm region due to overlap with the stagnant Phe spectrum, we do measure a difference of $\sim +0.16$ OD between EAS1 and EAS3 in the Pro-D:Phe solution at 240 nm—almost exactly double that of the Pro-D solution ($\sim +0.08$ OD), corroborating HPLC results that a greater population of Pre-D is present at long times in the mixture. Similarly, we find an increase at wavelengths greater than 300 nm in the mixture.

4.2. Potential Mechanisms for Photoprotection

Interestingly, the rate constant for Pro-D decay (EAS1) was identical in the Pro-D and Pro-D:Phe mixture. However, the rate associated with Pre-D decay was decreased by half, yielding a Pre-D population that persists for at least twice as long in the mixture (~ 100 min)—in agreement with an inspection of the difference absorption data and HPLC results. Given that the total illumination power was kept the same for both solutions, the most obvious explanation would be that the photostable Phe in solution is simply screening those blue wavelengths which readily convert Pre-D \rightarrow Tachy, ultimately slowing down that pathway since less light is available for Pre-D. If that were the only effect at work, however, one would expect an identical set of transients for all absorption features, only slower for the mixture. However, this is not the case. The transients shown in Figure 5b show similarities in curvature for 283 and 305 nm but non-negligible departures in curvature at 294 and 245 nm. More importantly, the rate constant for Pro-D decay (EAS1) should be affected in a similar fashion to Pre-D (EAS2) as screening by unaggregated Phe would be non-selective. Instead, only the decay of Pre-D is affected in an unambiguous way. These results warrant a broader discussion regarding the proximity and potential aggregation of the Pro-D and Phe species in solution and its effect on the kinetics observed.

It has been found that aggregation of Pro-D/Pre-D can significantly alter the photochemical product distribution, more often favoring the gZg -Pre-D form and thereby hindering Tachy formation [31,32]. These results were observed with a macromolecular substrate; however, where an abundance of hydrophobic and hydrophilic forces can bind Pro-D. Here, we explore the possibility of selective binding of Pro-D to a single Phe molecule in solution as a means to alter the kinetics and/or mechanism of the reaction. In order to do so, a computational survey of Pro-D $\bullet\bullet$ Phe structures was performed to quantify the Gibbs free energy of binding, $\Delta G_{\text{binding}}$, as an estimate of the likelihood of aggregation in solution. Out of approximately 40 structures computed with DFT, 8 yielded a $\Delta G_{\text{binding}} < 0$ and 4 of those yielded a $|\Delta G_{\text{binding}}| > RT$, suggesting the possibility of favorable binding at thermal equilibrium. Those structures, along with the individual Pro-D and Phe structures used to calculate $\Delta G_{\text{binding}}$, are shown in Figure 9. All of the dimer structures incorporate similar hydrogen bonding motifs with the ammonium group donating a hydrogen to the lone pairs of the Pro-D hydroxy group as well as the π system at the cyclohexadiene, and the carboxylate accepting the hydrogen from the Pro-D hydroxy. The differences between the structures are mainly associated with the alkyl tail of Pro-D, which alters the Phe approach slightly, yielding differences in H-bond distances and the proximity of the ammonium to the cyclohexadiene. Nevertheless, these calculations predict the possibility of Pro-D $\bullet\bullet$ Phe aggregation in solution, albeit with a binding free energy magnitude just greater than RT .

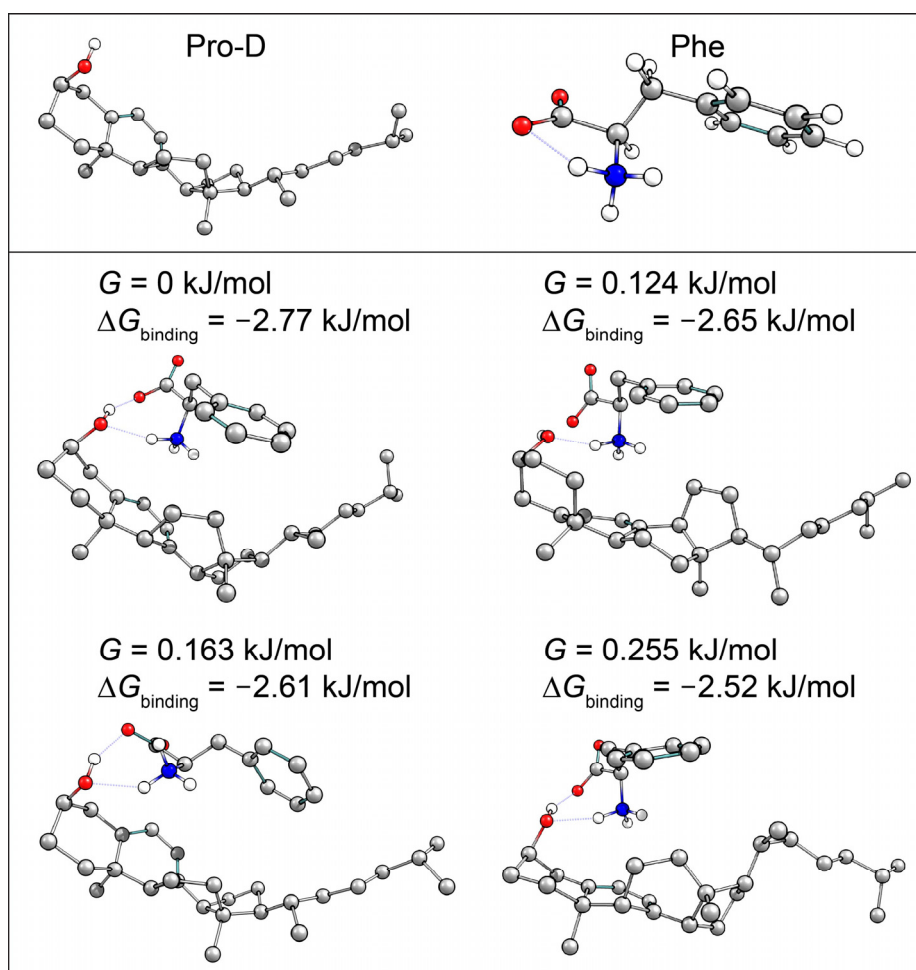


Figure 9. Calculated Pro-D and Phe structures (**top**), and Pro-D•••Phe structures with binding Gibbs energy magnitudes greater than RT (**bottom**). Hydrogens not involved in the hydrogen bonding network have been omitted for clarity.

With the chance for aggregation in solution, as predicted by DFT calculations, the effect of binding on the photochemical product yields must be considered. The prolonged existence of Pre-D in the mixture might suggest that steric hindrance due to Phe binding may increase the activation energy of the Tachy pathway, thereby decreasing its rate of formation. This interpretation is consistent with the Pro-D photolysis rate constant (EAS1) remaining unaffected, as bond cleavage should be minimally affected by the aggregation predicted by DFT. However, the dramatic kinetic effect of Phe is only observed when illuminating at 258 nm, remaining absent in 294 nm excitation experiments. This difference is significant since a structural argument for the difference in kinetics should be applicable regardless of excitation wavelength. This wavelength dependence, coupled with the Pre-D-specific variance in kinetics, suggests a more complex mechanism at work to explain this unique set of observations.

The computational prediction of stable Pro-D•••Phe dimers in solution at the very least highlights a general propensity for the two solute compounds to interact in solution, whether at short distances (Figure 9) or even at a longer range. Furthermore, Phe was selected as a candidate substrate for Pro-D both for its biological relevance and as a potential FRET donor, given its complementary absorption features to Pro-D. With that in mind, we must consider the possibility of a Phe \rightarrow Pro-D energy transfer pathway, which would be particularly active under 258 nm illumination, where Phe has its maximum absorbance. Introducing that new pathway to the mechanism would then allow for a higher Pro-D photolysis rate than if Phe was simply screening light from Pro-D, with the energy transfer

compensating for the lower Pro-D absorption rate. Notably, this hypothesis is consistent with the observation that the Pro-D decay rate remains constant with and without the presence of Phe. To test this hypothesis, FRET simulations were performed to address the efficiency and rate of energy transfer from Phe→Pro-D from short to long range in solution. In order to do so, first, the Förster spectral overlap, I , was determined by integrating the spectral overlap function between the Pro-D extinction spectrum, ϵ_A , and the area-normalized fluorescence spectrum of Phe, f_D [38,42,43].

$$I = \int_0^{\infty} \epsilon_A(\lambda) f_D(\lambda) \lambda^4 d\lambda. \quad (2)$$

Using an isotropic average as the structural orientation factor, κ , of $0.67^{1/2}$, we then calculated the Förster critical distance, R_0 , (the distance by which the energy transfer efficiency between Pro-D and Phe reaches 50%) by rearranging the FRET rate constant, k_{FRET} , in relation to R_0 : [38,42,43]

$$R_0 = \left(\frac{9000 \log(10) \kappa^2 I}{128 \pi^5 N_A n^4} \right)^{1/6} \quad (3)$$

where N_A is Avogadro's number and n is the refractive index of the solvent (methanol). R_0 was found to be 3.10 nm for the Pro-D-Phe pair, and Figure 10 shows the FRET efficiency, η_{FRET} , with Phe-Pro-D distance in solution calculated as: [42,43]

$$\eta_{\text{FRET}} = \frac{1}{1 + \left(\frac{R}{R_0} \right)^6} \quad (4)$$

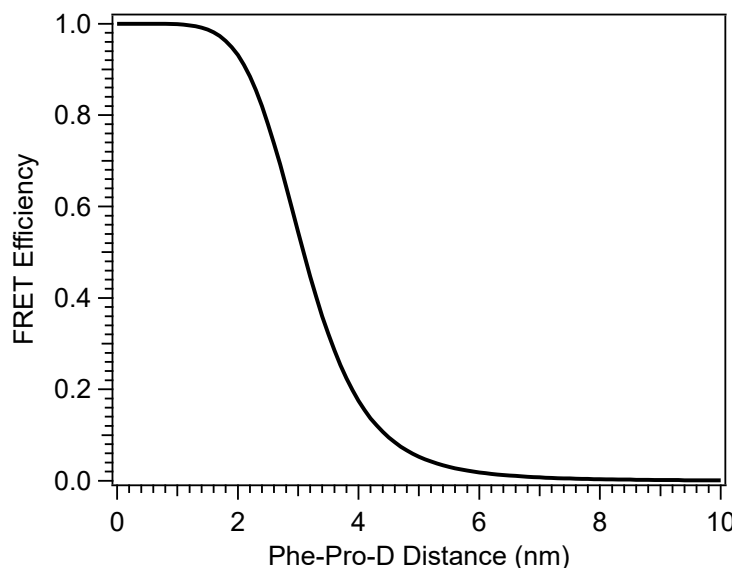


Figure 10. Efficiency of energy transfer between Phe and Pro-D in a methanol solution calculated by Förster resonance energy transfer theory.

The FRET simulation shown in Figure 10 suggests that energy transfer from Phe to Pro-D is possible within a distance of ~8 nm. Briefly ignoring the possibility of short-range aggregation, the average distance between the two molecules in solution can be estimated by considering their molar concentrations and assuming a random distribution of non-interacting molecules. That distance is found to be ~8.5 nm—near the edge of the predicted range for FRET to be non-negligible. Specifically, the efficiency of energy transfer at that distance is 0.23%, according to Figure 10, implying that a random distribution of Phe and Pro-D will not provide access to the energy transfer pathway at the level of compensating for the nearly 0.5 OD difference in available light intensity for Pro-D excitation due to

screening by Phe. Thus, the two molecules are assumed to be engaged in intermolecular interactions to draw them together in solution in accordance with the $\Delta G_{\text{binding}}$ calculated for the dimer structures. We note that at a very short range, one might expect some minor distortions of the absorption features of either Phe or Pro-D; however, the extent of overlap and broadening in the spectrum of the mixture prohibits a close analysis. In addition, Förster theory addresses the long-range resonance energy transfer phenomenon, while at short range, significant mixing of the electronic character of the dimer excited states coupled with Dexter energy transfer becomes prominent. However, the electronic chromophores within the calculated dimer structures are nearly 7 Å apart to accommodate the hydrogen bonding cycle at the termini of the two molecules. At that distance, alterations of the electronic character of the two and their absorption spectra should be minimal and likely undetectable.

Reflecting on these favorable structural factors of a Pro-D $\bullet\bullet\bullet$ Phe aggregate, and the passive and active effects observed by bringing a photostable aromatic amino acid in proximity to Pro-D, one might anticipate similar effects *in vivo* where Pro-D is in proximity to aromatic residues of epidermal proteins such as keratin. In fact, the total keratin concentration [44] and Pro-D concentration [4] in the skin is comparable to the Phe and Pro-D concentrations used here, suggesting significant potential for this type of photoprotection within the skin since each protein contains multiple aromatic residues. In this way, the vitamin D formation from an actively and passively photoprotected Pre-D population would be significantly more efficient. These insights can be tailored to other photochemical reactions that yield a significant wavelength dependence, where a carefully designed donor substrate may steer the photochemistry to the desired products without losses in absorption efficiency due to passive screening.

5. Conclusions

The effects of proximal Phe on the photochemistry of Pro-D was investigated through time-resolved absorption spectroscopy, in tandem with global kinetic analysis, HPLC analysis of photochemical product ratios, and computational predictions of aggregation. Illuminating solutions of Pro-D and a Pro-D:Phe mixture at 294 nm resulted in nearly identical evolution of the absorption spectrum and product branching in both solutions. Importantly, illumination at 294 nm almost exclusively led to the excitation of Pro-D at the red edge of its absorption spectrum, while excluding excitation of Phe due to its blue-shifted spectrum. However, illuminating the two solutions at 258 nm at the peak of the Phe absorption spectrum overlapped with the blue-most absorption of Pro-D, revealed significant differences in both the absorption spectrum evolution and product concentrations upon the incorporation of Phe in solution.

Global analysis, utilizing a three-component sequential model, yielded an excellent fit to the time-resolved absorption spectra, and only the time scale pertaining to the decay of Pre-D was altered between a Pro-D solution and a Pro-D:Phe mixture. Specifically, the incorporation of Phe significantly prolonged the Pre-D intermediate, yielding a time constant nearly twice that of a Pro-D solution. Surprisingly, however, the Pro-D decay timescale was unchanged by the presence of Phe, hinting at a more complex mechanism of photoprotection by Phe compared to simple light screening.

Pro-D $\bullet\bullet\bullet$ Phe H-bonded dimer structures were calculated with DFT to investigate whether the pair would show favorable interactions, leading to potential aggregation in solution. Several structures were predicted to be stable at room temperature, indicating likely non-random pairwise interactions between the two molecules in solution, lending them the ability to undergo resonance energy transfer. The complementary absorption and fluorescence features of Phe relative to Pro-D particularly enable the addition of an energy transfer event from Phe \rightarrow Pro-D, triggering the ring-opening reaction leading to Pre-D. This added pathway ultimately compensates for the difference in absorption by Pro-D at those blue wavelengths, yielding a similar concentration of excited Pro-D despite the significant screening by Phe in that region. Importantly, since the Phe absorption spectrum spans the

wavelengths that generate high concentrations of undesired products such as Tachy, and its fluorescence spectrum yields a spectral overlap toward the red region of the Pro-D absorption, it serves as an ideal energy transfer donor to maximize an intermediate population of Pre-D. Therefore, we propose that Phe exhibits dual photoprotection properties for Pro-D. Firstly, it screens parasitic wavelengths that render undesired photochemical products from Pre-D, such as Tachy, while simultaneously down-converting absorbed energy to energies more amenable to Pro-D excitation, leading to a greater overall Pre-D yield.

Supplementary Materials: The following supporting information can be downloaded at: <https://www.mdpi.com/article/10.3390/photochem3040029/s1>, Figure S1: Spectra of excitation source used in the photochemistry experiments reported; Figure S2: HPLC-DAD chromatogram showing elution times of various species in a reaction mixture. Each peak is labeled with the full DAD absorption spectrum enabling the identification of each elution; Figure S3: HPLC-DAD chromatograms (solid) taken at a detection wavelength of 280 nm for Pro-D and Pro-D:Phe mixtures following 294 and 258 nm illumination. The left column shows a three-gaussian fit function (dashed) along with residuals between the fit and experiment. The right column shows the three individual gaussians fit against their respective elution; Figure S4: Experimental absorbance transients taken from a (a) Pro-D and (b) Pro-D:Phe mixture at 245 nm (blue), 283 nm (green), 294 nm (black), and 305 nm (red) detection wavelengths following 258 nm light exposure. Solid lines are from global spectra fitting of the data; atomic coordinates of calculated Pro-D, Phe, and Pro-D••Phe structures.

Author Contributions: Conceptualization, G.A.O. and J.C.D.; Methodology and Analysis, G.A.O., J.S.M. and J.C.D.; Data Curation, G.A.O. and J.S.M.; Funding Acquisition, G.A.O. and J.C.D.; Writing—Original Draft Preparation, G.A.O. and J.C.D.; Writing—Review and Editing, G.A.O., J.S.M. and J.C.D. All authors have read and agreed to the published version of the manuscript.

Funding: This research was funded by the Southern Utah University Faculty Scholarly Support Fund (FSSF) and Walter Maxwell Gibson Research Fellowship.

Data Availability Statement: Data may be made available by J.C.D. upon request by email.

Acknowledgments: The authors gratefully acknowledge the SUU Faculty Scholarly Support Fund for supporting this work, as well as the Walter Maxwell Gibson endowment for supporting G.A.O. and J.S.M. in their research. The authors also thank Kim Weaver for assistance and discussions regarding HPLC.

Conflicts of Interest: The authors declare no conflict of interest.

References

1. Laird, E.; Ward, M.; McSorley, E.; Strain, J.J.; Wallace, J. Vitamin D and Bone Health; Potential Mechanisms. *Nutrients* **2010**, *2*, 693–724. [[CrossRef](#)] [[PubMed](#)]
2. You, H.; Shin, H.R.; Song, S.; Ly, S.Y. Vitamin D Intake and Bone Mineral Density in Korean Adults: Analysis of the 2009–2011 Korea National Health and Nutrition Examination Survey. *Nutr. Res. Pract.* **2022**, *16*, 775–788. [[CrossRef](#)]
3. Christodoulou, S.; Goula, T.; Ververidis, A.; Drosos, G. Vitamin D and Bone Disease. *BioMed Res. Int.* **2013**, *2013*, 396541. [[CrossRef](#)]
4. Holick, M.F.; MacLaughlin, J.A.; Clark, M.B.; Holick, S.A.; Potts, J.T.; Anderson, R.R.; Blank, I.H.; Parrish, J.A.; Elias, P. Photosynthesis of Previtamin D3 in Human Skin and the Physiologic Consequences. *Science* **1980**, *210*, 203–205. [[CrossRef](#)]
5. Huiberts, L.M.; Smolders, K.C.H.J. Effects of Vitamin D on Mood and Sleep in the Healthy Population: Interpretations from the Serotonergic Pathway. *Sleep Med. Rev.* **2021**, *55*, 101379. [[CrossRef](#)]
6. Wilkins, C.H.; Sheline, Y.I.; Roe, C.M.; Birge, S.J.; Morris, J.C. Vitamin D Deficiency Is Associated with Low Mood and Worse Cognitive Performance in Older Adults. *Am. J. Geriatr. Psychiatry* **2006**, *14*, 1032–1040. [[CrossRef](#)]
7. Tsugawa, N. Cardiovascular Diseases and Fat Soluble Vitamins: Vitamin D and Vitamin K. *J. Nutr. Sci. Vitaminol. (Tokyo)* **2015**, *61*, S170–S172. [[CrossRef](#)]
8. Holick, M.F. Vitamin D: A Millenium Perspective. *J. Cell. Biochem.* **2003**, *88*, 296–307. [[CrossRef](#)]
9. Chen, T.C.; Chimeh, F.; Lu, Z.; Mathieu, J.; Person, K.S.; Zhang, A.; Kohn, N.; Martinello, S.; Berkowitz, R.; Holick, M.F. Factors That Influence the Cutaneous Synthesis and Dietary Sources of Vitamin D. *Arch. Biochem. Biophys.* **2007**, *460*, 213–217. [[CrossRef](#)]
10. Vieth, R. Vitamin D Supplementation, 25-Hydroxyvitamin D Concentrations, and Safety. *Am. J. Clin. Nutr.* **1999**, *69*, 842–856. [[CrossRef](#)]
11. Holick, M.F. Medical Progress: Vitamin D Deficiency. *N. Engl. J. Med.* **2007**, *357*, 266–281. [[CrossRef](#)] [[PubMed](#)]

12. Xu, G.; Salen, G.; Shefer, S.; Ness, G.C.; Chen, T.S.; Zhao, Z.; Tint, G.S. Reproducing Abnormal Cholesterol Biosynthesis as Seen in the Smith-Lemli-Opitz Syndrome by Inhibiting the Conversion of 7-Dehydrocholesterol to Cholesterol in Rats. *J. Clin. Investig.* **1995**, *95*, 76–81. [CrossRef] [PubMed]
13. Borch, R.F.; Yamamoto, J.K. Photoconversion of 7-Dehydrocholesterol to Vitamin D3 in Synthetic Phospholipid Bilayers. *Biochemistry* **1985**, *24*, 3338–3344.
14. Valencia, A.; Rajadurai, A.; Carle, A.B.; Kochevar, I.E. 7-Dehydrocholesterol Enhances Ultraviolet A-Induced Oxidative Stress in Keratinocytes: Roles of NADPH Oxidase, Mitochondria, and Lipid Rafts. *Free Radic. Biol. Med.* **2006**, *41*, 1704–1718. [CrossRef] [PubMed]
15. Dembitsky, V.M. In Silico Prediction of Steroids and Triterpenoids as Potential Regulators of Lipid Metabolism. *Mar. Drugs* **2021**, *19*, 650. [CrossRef] [PubMed]
16. Tian, X.Q.; Chen, T.C.; Matsuoka, L.Y.; Wortsman, J.; Holick, M.F. Kinetic and Thermodynamic Studies of the Conversion of Previtamin D3 to Vitamin D3 in Human Skin. *J. Biol. Chem.* **1993**, *268*, 14888–14892. [CrossRef]
17. Tapavicza, E.; Meyer, A.M.; Furche, F. Unravelling the Details of Vitamin D Photosynthesis by Non-Adiabatic Molecular Dynamics Simulations. *Phys. Chem. Chem. Phys.* **2011**, *13*, 20986–20998. [CrossRef]
18. Solis-Urra, P.; Cristi-Montero, C.; Romero-Parra, J.; Zavala-Crichton, J.P.; Saez-Lara, M.J.; Plaza-Diaz, J. Passive Commuting and Higher Sedentary Time Is Associated with Vitamin D Deficiency in Adult and Older Women: Results from Chilean National Health Survey 2016–2017. *Nutrients* **2019**, *11*, 300. [CrossRef]
19. Havinga, E.; Schlatmann, J.L.M.A. Remarks on the Specificities of the Photochemical and Thermal Transformations in the Vitamin D Field. *Tetrahedron* **1961**, *16*, 146–152. [CrossRef]
20. Havinga, E.; de Kock, R.J.; Rappoldt, M.P. The Photochemical Interconversions of Provitamin D, Lumisterol, Previtamin D and Tachysterol. *Tetrahedron* **1960**, *11*, 276–284. [CrossRef]
21. Tang, K.-C.; Rury, A.; Orozco, M.B.; Egendorf, J.; Spears, K.G.; Sension, R.J. Ultrafast Electrocyclic Ring Opening of 7-Dehydrocholesterol in Solution: The Influence of Solvent on Excited State Dynamics. *J. Chem. Phys.* **2011**, *134*, 104503. [CrossRef] [PubMed]
22. Meyer-Ilse, J.; Akimov, D.; Dietzek, B. Ultrafast Circular Dichroism Study of the Ring Opening of 7-Dehydrocholesterol. *J. Phys. Chem. Lett.* **2012**, *3*, 182–185. [CrossRef]
23. Arruda, B.C.; Sension, R.J. Ultrafast Polyene Dynamics: The Ring Opening of 1,3-Cyclohexadiene Derivatives. *Phys. Chem. Chem. Phys.* **2014**, *16*, 4439–4455. [CrossRef] [PubMed]
24. Snyder, J.W., Jr.; Curchod, B.F.E.; Martinez, T.J. GPU-Accelerated State-Averaged Complete Active Space Self-Consistent Field Interfaced with Ab Initio Multiple Spawning Unravels the Photodynamics of Provitamin D3. *J. Phys. Chem. Lett.* **2016**, *7*, 2444–2449. [CrossRef] [PubMed]
25. Smith, B.D.; Spears, K.G.; Sension, R.J. Probing the Biexponential Dynamics of Ring-Opening in 7-Dehydrocholesterol. *J. Phys. Chem. A* **2016**, *120*, 6575–6581. [CrossRef] [PubMed]
26. Jacobs, H.J.C.; Havinga, E. Photochemistry of Vitamin D and Its Isomers and of Simple Trienes. *Adv. Photochem.* **1979**, *11*, 305–373.
27. Cisneros, C.; Thompson, T.; Baluyot, N.; Smith, A.C.; Tapavicza, E. The Role of Tachysterol in Vitamin D Photosynthesis—a Non-Adiabatic Molecular Dynamics Study. *Phys. Chem. Chem. Phys.* **2017**, *19*, 5763–5777. [CrossRef] [PubMed]
28. Norval, M.; Björn, L.O.; De Gruijl, F.R. Is the Action Spectrum for the UV-Induced Production of Previtamin D3 in Human Skin Correct? *Photochem. Photobiol. Sci.* **2010**, *9*, 11–17. [CrossRef]
29. Maessen, P.A.; Jacobs, H.J.C.; Cornelisse, J.; Havinga, E. Photochemistry of Previtamin D3 at 92 K; Formation of an Unstable Tachysterol Rotamer. *Angew. Chem. Int. Ed. Engl.* **1983**, *22*, 994–1004. [CrossRef]
30. Arruda, B.C.; Peng, J.; Smith, B.; Spears, K.G.; Sension, R.J. Photochemical Ring-Opening and Ground State Relaxation in α -Terpinene with Comparison to Provitamin D3. *J. Phys. Chem. B* **2013**, *117*, 4696–4704. [CrossRef]
31. Dmitrenko, O.; Orlova, T.; Terenetskaya, I. Medium Controlled Photochemistry of Provitamin D: From Solutions to Liquid Crystals. *J. Mol. Liq.* **2018**, *267*, 428–435. [CrossRef]
32. Sofferma, D.L.; Konar, A.; Mastron, J.N.; Spears, K.G.; Cisneros, C.; Smith, A.C.; Tapavicza, E.; Sension, R.J. Probing the Formation and Conformational Relaxation of Previtamin D3 and Analogs in Solution and in Lipid Bilayers. *J. Phys. Chem. B* **2021**, *125*, 10085–10096. [CrossRef]
33. Holick, M.F.; Tian, X.Q.; Allen, M. Evolutionary Importance for the Membrane Enhancement of the Production of Vitamin D3 in the Skin of Poikilothermic Animals. *Proc. Natl. Acad. Sci. USA* **1995**, *92*, 3124–3126. [CrossRef]
34. Saltiel, J.; Cires, L.; Turek, A.M. Conformer-Specific Photoconversion of 25-Hydroxytachysterol to 25-Hydroxyprevitamin D3: Role in the Production of Vitamin Ds. *J. Am. Chem. Soc.* **2003**, *125*, 2866–2867. [CrossRef] [PubMed]
35. Orlova, T.N.; Terenetskaya, I.P. Specific Features of Photoisomerization of Provitamin D3 in a Nematic Liquid Crystal. *Opt. Spectrosc.* **2006**, *100*, 584–589. [CrossRef]
36. Terenetskaya, I.P.; Perminova, O.G.; Yeremenko, A.M. Photoisomerization of Provitamin D in Dispersive Systems. *J. Mol. Struct.* **1990**, *219*, 359–364. [CrossRef]
37. Tian, X.Q.; Holick, M.F. A Liposomal Model That Mimics the Cutaneous Production of Vitamin D3: Studies of the Mechanism of the Membrane-Enhanced Thermal Isomerization of Previtamin D3 to Vitamin D3. *J. Biol. Chem.* **1999**, *274*, 4174–4179. [CrossRef]
38. Scholes, G.D. Long-Range Resonance Energy Transfer in Molecular Systems. *Annu. Rev. Phys. Chem.* **2003**, *54*, 57–87. [CrossRef]

39. Snellenburg, J.J.; Laptenok, S.P.; Seger, R.; Mullen, K.M.; van Stokkum, I.H.M. Glotaran: A Java-Based Graphical User Interface for the R Package TIMP. *J. Stat. Softw.* **2012**, *49*, 1–22. [[CrossRef](#)]
40. Gaussian 16, R.B. 01; Gaussian 16; Gaussian, Inc.: Wallingford, CT, USA, 2016.
41. Mohamadi, F.; Richards, N.G.J.; Guida, W.C.; Liskamp, R.; Lipton, M.; Caufield, C.; Chang, G.; Hendrickson, T.; Still, W.C. Macromodel—An Integrated Software System for Modeling Organic and Bioorganic Molecules Using Molecular Mechanics. *J. Comput. Chem.* **1990**, *11*, 440–467. [[CrossRef](#)]
42. Olaya-Castro, A.; Scholes, G.D. Energy Transfer from Förster–Dexter Theory to Quantum Coherent Light-Harvesting. *Int. Rev. Phys. Chem.* **2011**, *30*, 49–77. [[CrossRef](#)]
43. Mirkovic, T.; Ostroumov, E.E.; Anna, J.M.; van Grondelle, R.; Govindjee; Scholes, G.D. Light Absorption and Energy Transfer in the Antenna Complexes of Photosynthetic Organisms. *Chem. Rev.* **2017**, *117*, 249–293. [[CrossRef](#)] [[PubMed](#)]
44. Feng, X.; Zhang, H.; Margolick, J.B.; Coulombe, P.A. Keratin Intracellular Concentration Revisited: Implications for Keratin Function in Surface Epithelia. *J. Investigig. Dermatol.* **2013**, *133*, 850–853. [[CrossRef](#)] [[PubMed](#)]

Disclaimer/Publisher’s Note: The statements, opinions and data contained in all publications are solely those of the individual author(s) and contributor(s) and not of MDPI and/or the editor(s). MDPI and/or the editor(s) disclaim responsibility for any injury to people or property resulting from any ideas, methods, instructions or products referred to in the content.